Vol. 717: 107–126, 2023
https://doi.org/10.3354/meps14373

MARINE ECOLOGY PROGRESS SERIES
Mar Ecol Prog Ser

Published August 24

Effects of migrating mesopelagic fishes on the biological carbon pump

Dag L. Aksnes[1,*], Anita S. Løtvedt[1], Christian Lindemann[1], Maria Ll. Calleja[2], Xosé Anxelu G. Morán[3], Stein Kaarvedt[4], T. Frede Thingstad[1]

[1]Department of Biological Sciences, University of Bergen, 5020 Bergen, Norway
[2]Max Planck Institute for Chemistry, 55128 Mainz, Germany
[3]Instituto Español de Oceanografia, 33212 Gijón, Spain
[4]Department of Biosciences, University of Oslo, 0316 Oslo, Norway

ABSTRACT: Mesopelagic fishes and invertebrates contribute to the biological carbon pump (BCP) through direct and indirect effects on the gravitational, diffusive, and migrant (active) fluxes. Here, we analyzed the effect of these organisms on total carbon export and sequestration using an idealized depth-resolved food-web model. We constrained a baseline scenario with observations from the Red Sea where mesopelagic fishes perform extensive diel vertical migration (DVM), presumably making them particularly important in carbon export. Our results are consistent with previous studies suggesting that mesopelagic fishes fuel a hotspot of heterotrophic activity in the mesopelagic zone of the Red Sea. While the supply of new nutrients to the euphotic zone is of first order in framing total carbon export and sequestration, we found 2 modulating effects of fish DVM. First, DVM enhances carbon sequestration because active carbon flux attenuates less than the gravitational and diffusive fluxes, and also because migrators fuel the gravitational flux deep into the mesopelagic zone. Secondly, through microbial food-web cascades, fish predation affects the relative contribution of the active and the passive fluxes with non-linear, less intuitive consequences for carbon export and sequestration. These food-web cascades involve a surprisingly large variation in the depth of the euphotic zone that is associated with a 'diatom nutrient trap' at the bottom of the euphotic zone.

KEY WORDS: Diel vertical migration · DVM · Fish · Microbial food web · Cascade · Carbon flux · Subtropical ocean · Red Sea

1. INTRODUCTION

The ocean plays a critical role in controlling the atmospheric concentration of CO_2 and in regulating the climate on Earth (Honjo et al. 2014). Biologically driven net drawdown of particulate (POC) and dissolved organic carbon (DOC) is commonly termed the biological carbon pump (BCP). The BCP is driven by a complex set of physical, biological, and biogeochemical processes involving marine biota from microbes to metazoans. Sinking of POC, mixing and convection of POC and DOC, and vertical migration of invertebrates and fishes contribute to the BCP. The DOC, and most of the POC (unless buried in bottom sediments), are remineralized as CO_2 or degraded to recalcitrant DOC in the water column. The deeper this remineralization occurs, the longer the carbon is sequestered away from potential exchange with the atmosphere (Boyd et al. 2019). Concerning metazoans, most emphasis has been on zooplankton (Turner 2015, Nowicki et al. 2022, Stukel et al. 2022), but the influence of fish and fisheries on the BCP are increasingly being addressed (Getzlaff & Oschlies

*Corresponding author: dag.aksnes@uib.no

Publisher: Inter-Research · www.int-res.com

2017, Mariani et al. 2020, Bianchi et al. 2021, Saba et al. 2021, Cavan & Hill 2022).

Many fishes and invertebrates perform diel vertical migration (DVM), spending part of their time in the epipelagic and part of their time in the mesopelagic. If these organisms feed more in the epipelagic than in the mesopelagic, they contribute to increased downward carbon flux and sequestration (Bianchi et al. 2013, 2021, Davison et al. 2013, Irigoien et al. 2014, Saba et al. 2021). This is because carbon ingested as food in the epipelagic is transported by these fish to mesopelagic depths, where carbon is respired as CO_2, excreted as DOC, defecated as POC, or consumed by piscivores. This transport is referred to as the migrant (Nowicki et al. 2022) or active (Belcher et al. 2019) carbon flux. There are large uncertainties, however, on how much mesopelagic fishes contribute to the BCP. This is due to lack of knowledge about species biology and composition (Caiger et al. 2021, Saba et al. 2021), abundances (Kaartvedt et al. 2012, Irigoien et al. 2014, Proud et al. 2019), migration amplitude, and the proportion of populations taking part in the migrations (Klevjer et al. 2016). Another challenge in assessing the role of DVM in carbon sequestration is that migration also affects the gravitational (sinking of POC) and diffusive (POC and DOC that are mixed vertically) fluxes directly (e.g. by defecation) and indirectly through food-web effects.

Here, we used an idealized ecosystem model to analyze the effects of mesopelagic organisms and their DVM on carbon export and sequestration. The kernel of this model is the minimum microbial food-web model (MinMod; Fig. 1) conceptually framed by Thingstad & Rassoulzadegan (1999) and further developed in association with mesocosm perturbation experiments (reviewed by Thingstad 2020). MinMod links carbon, phosphorus, and silicate fluxes to

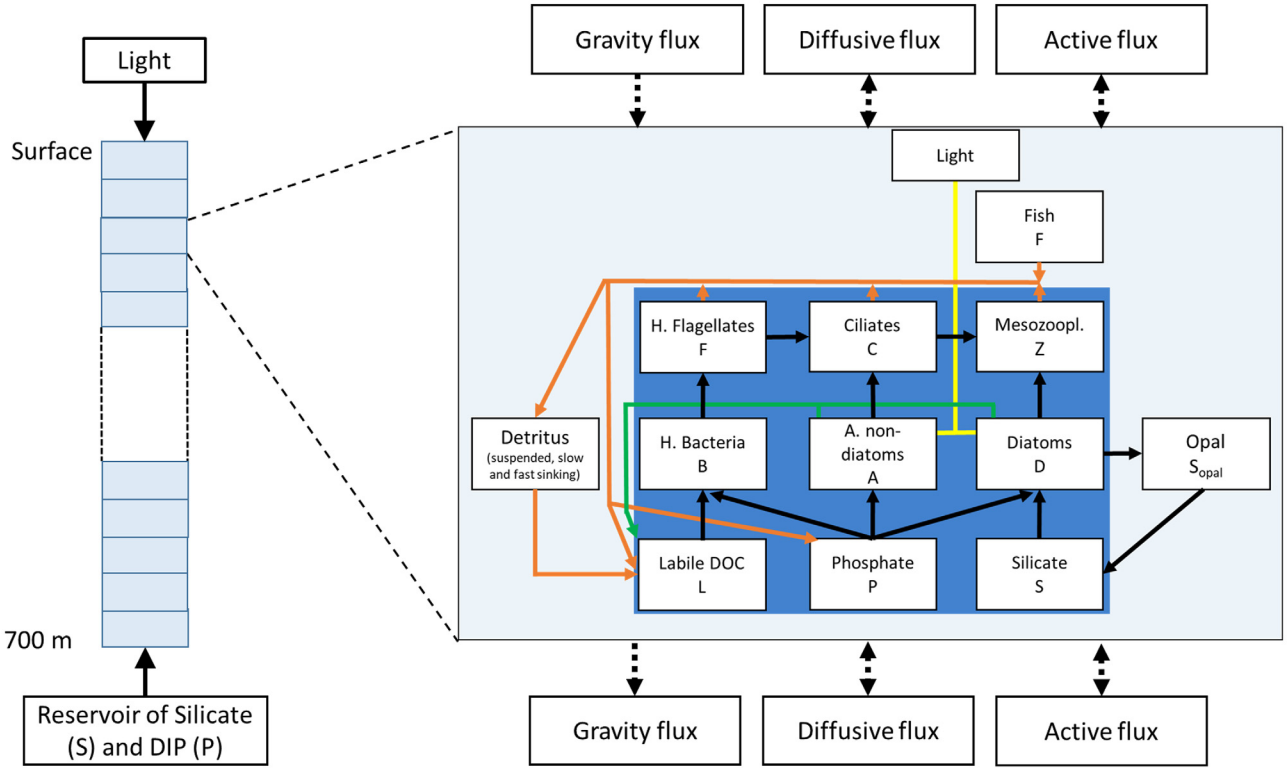

Fig. 1. Relationship between the original MinMod (Thingstad 2007, Thingstad et al. 2020) and our depth-resolved MinMod. The original MinMod includes 9 state variables: labile dissolved organic carbon (DOC) (L), free silicate (S), dissolved inorganic phosphate (P), heterotrophic bacteria (B), autotrophic non-diatoms (A), diatoms (D), heterotrophic flagellates (H), ciliates (C), and mesozooplankton (M). In our model, autotrophic non-diatoms reflect prokaryotic photosynthesis as well as flagellate photosynthesis (see Section 2.2). In our depth-resolved model, we included mesozooplanktivorous fish (F), opal (S_{opal}), and detritus. Detritus contains 3 subgroups: suspended, slow-sinking, and fast-sinking detritus (see Fig. S2 in the Supplement at www.int-res.com/suppl/m717p107_supp.pdf). We also included light-limited autotrophic growth (indicated by the yellow line) and photosynthetic overflow resulting in labile DOC (green line). The brown lines indicate dissolved and particulate losses from the heterotrophic organisms and from detritus. Respiratory carbon loss is accounted for in the model but not indicated in the illustration (see Fig. S2)

the size spectrum of biogenic particles in the euphotic zone (Thingstad & Rassoulzadegan 1999). It is characterized by 3 competing microbial pathways that affect degradation of dissolved organic matter, ocean carbon sequestration, and food production for higher trophic levels (Thingstad & Rassoulzadegan 1999). Important in the present context are cascading effects from mesozooplankton on the structure of the microbial food web. As the 3 microbial pathways from dissolved inorganic phosphorus (DIP) to mesozooplankton have different lengths (Fig. 1), variations in mesozooplankton affect the balance between these microbial pathways. Both experimental and theoretical studies (Wollrab & Diehl 2015, Zeldis & Décima 2020, Thingstad 2020) have found that mesozooplankton abundance, through trophic cascades, modulates this balance and thereby the biogeochemical functions in the microbial food web. In the present study, we depth-resolved MinMod and extended the model with mesopelagic fishes feeding on mesozooplankton. Mesopelagic fishes are (by definition) inhabitants of the mesopelagic zone, although they may spend substantial time feeding in the epipelagic. Thus, they are predators on the mesozooplankton in the epipelagic zone, implying potential top-down cascading effects on the euphotic microbial food web and its biogeochemical function.

We used observations from the Red Sea to constrain a baseline scenario serving as the starting point of our analysis. The acoustic scattering layers of the Red Sea show very pronounced and persistent DVM throughout the year, and where the entire stock of mesopelagic fishes apparently takes part in this DVM (Klevjer et al. 2012, Dypvik & Kaartvedt 2013, Kaartvedt et al. 2019b). Furthermore, there is a lack of migrations in the mesozooplankton (Dypvik & Kaartvedt 2013), suggesting that mesopelagic fishes, potentially in association with larger zooplankton such as krill (Seibel et al. 2016, Wiebe et al. 2016), are responsible for the active carbon flux. Scarcity of mesozooplankton in the mesopelagic zone in combination with high temperature and low dissolved oxygen might be a reason for why the entire population of mesopelagic fishes appears to participate in the daily migrations in the Red Sea. Importance of fish migrations and their associated active carbon flux are indicated by previous studies revealing a hotspot of heterotrophic prokaryotes in the mesopelagic zone likely being stimulated by fish excretion at their mesopelagic daytime depth (Calleja et al. 2018, Morán et al. 2022).

The Red Sea is like the subtropical ocean in being highly transparent (Overmans & Agustí 2019), oligotrophic, and permanently stratified, and having acoustic scattering layers with pronounced DVM patterns (Klevjer et al. 2016). One difference, however, is the uniquely warm, >21°C, mesopelagic zone of the Red Sea. High temperature suggests high remineralization rates and consequently high attenuation of the gravitational carbon flux (Marsay et al. 2015, Mazuecos et al. 2015). Combined with the lack of DVM in the mesozooplankton, this suggests that mesopelagic fishes injecting carbon deep into the mesopelagic zone might be more important for carbon export here than elsewhere, and the Red Sea might potentially serve as a model for assessing maximal impact of mesopelagic fishes in the BCP. More generally, using the Red Sea baseline scenario as a reference, we investigated how the 3 main microbial pathways and the associated carbon export and sequestration change with alterations in productivity as determined bottom-up by the input of new nutrients (Eppley & Peterson 1979) and top-down by cascade effects on the food web (Getzlaff & Oschlies 2017, Thingstad 2020). These bottom-up and top-down forcings are set by water-column mixing parameterized as turbulent diffusivity and by the mortality and migration of mesopelagic fishes.

2. MATERIALS AND METHODS

2.1. Red Sea observations

We assumed a quasi-steady state situation representing the summer and autumn period of the Red Sea. Thus, we did not consider the seasonal variation that is associated with a weakening of the density stratification in early spring (Calleja et al. 2019, Kheireddine et al. 2020, Torfstein et al. 2020, López-Sandoval et al. 2021). To characterize the quasi-steady state, we used observations from August and September 2015 from Calleja et al. (2019) at station KAEC (22.47° N, 39.03° E). At that time, there was a pronounced density stratification in the upper ~150 m (Fig. S1A in the Supplement at www.int-res.com/articles/suppl/m717p107_supp.pdf). Surface temperature was just above 30°C and dropped to 22°C at 200 m depth and remained higher than 21°C down to 700 m depth (Fig. S1B). Dissolved oxygen concentration was 2–3 ml l^{-1} in the upper 150 m and dropped to 0.4–0.5 ml l^{-1} in the mesopelagic (Fig. S1C). The euphotic depth corresponded to 77 and 100 m (Fig. S1D) according to the definitions of 0.5% (Wu et al. 2021) and 0.1% (Buesseler et al. 2020) light penetration, respectively. A deep chlorophyll maximum was located above 100 m (Fig. S1E), with the steepest nutri-

cline below (Fig. S1F). DOC and heterotrophic bacteria had the highest concentrations in the euphotic zone (~80 µmol l^{-1} and ~5 × 10^5 cells ml^{-1}, respectively) dropping to ~50 µmol l^{-1} and ~1 × 10^5 cells ml^{-1} in the mesopelagic zone (Fig. S1G,H). Mesozooplankton abundance was highest (~300–700 ind. m^{-3}) in the euphotic zone and very low in the mesopelagic zone (<35 ind. m^{-3}) both day and night (Fig. S1I), indicating absence of DVM in the mesozooplankton. Acoustic backscatter, which we used as a proxy for the relative vertical distribution and associated DVM in fish, was mainly found above 150 m at night, while being strong between 300 and 600 m in the daytime (Fig. S1J).

2.2. Food-web model

Text S1 contains a complete description of the model. The kernel of the model is the minimum microbial food-web model, MinMod (see Section 1). The organism groups of the model are aggregates of species reflecting different size groups and functions; for example, the division into heterotrophic and autotrophic groups is functional since true organisms might belong to both groups by mixotrophy. The original MinMod includes 9 state-variables (Fig. 1; Table S1). Dissolved inorganic phosphate (DIP) is the limiting mineral nutrient for the autotrophs and heterotrophic bacteria, which accords with findings in the Red Sea (Silva et al. 2019, López-Sandoval et al. 2021). We also note that use of phosphorus as a limiting mineral nutrient simplifies modeling because phosphorus, in contrast to nitrogen, is not in exchange with gaseous reservoirs and further does not exist in multiple bio-accessible inorganic forms. DIP enters the food web through uptake by 2 autotrophic groups and by heterotrophic bacteria. Besides DIP, the availability of silicate and labile DOC (l-DOC) limits the growth of diatoms and heterotrophic bacteria, respectively. Prokaryotic photosynthesis is not explicitly represented in MinMod, and here we assumed that this carbon fixation is reflected by a non-diatom autotrophic group (Fig. 1). Furthermore, the model does not explicitly differentiate between labile and semi-labile DOC, and the actual lability is set by a coefficient defining the bacterial affinity for l-DOC (see Section 2.3). Thus, our l-DOC state variable reflects both labile and semi-labile DOC. The model accounts for photosynthetic carbon overflow (Thingstad et al. 2007, Thornton 2014) resulting in extracellular release of l-DOC. This implies that more carbon is fixed and instantaneously excreted as l-DOC than by the Redfield ratio assumed for autotrophic growth and biomass. In the model, this l-DOC is either respired by bacteria or enters the food web through heterotrophic flagellates feeding on bacteria (Fig. 1). Except for heterotrophic bacteria, which have a molar C:P ratio of 50 in the model (Thingstad et al. 2007), the C:P ratio of the organism groups is 106 according to the Redfield ratio.

The original MinMod is formulated as a box model of the euphotic zone where light is considered non-limiting for autotrophic growth. In our depth-resolved version, we have introduced light, self-shading, and light-limited growth for the autotrophs (see Text S1). Following the categorization used in marine snow-catcher experiments (Riley et al. 2012, Giering et al. 2016, Baker et al. 2017), we added 3 state variables for detritus (fast-sinking, slow-sinking, and suspended detritus, Fig. 1; Fig. S2), which contain POC and particulate organic phosphorus (POP). We also included a zooplanktivore referred to as 'fish', feeding on mesozooplankton (Fig. 1). Because fish are the only predators on mesozooplankton, the fish state variable represents all feeders on mesozooplankton. In nature, these will also include invertebrates. It should also be noted that the mesozooplankton of our idealized model feeds exclusively on the ciliates and the diatoms, while in nature mesozooplankton is a diverse group feeding on other organism groups as well as on detritus.

Except for fish (see below), changes in the state variables (X_i; Table S1) as a function of time (t) and depth (z) are represented by 1 partial differential equation for each state variable:

$$\frac{\partial X_i}{\partial t} = B(X_i) + \frac{\partial}{\partial z}\kappa\frac{\partial X_i}{\partial z} - v_{X_i}\frac{\partial X_i}{\partial z} \quad (1)$$

Here, $B(X_i)$ are the biological source and sink terms (Tables S2–S4), κ is a coefficient for turbulent diffusivity, and v_{X_i} is the gravitational sinking rate, which is non-zero only for slow- and fast-sinking detritus. We have represented sinking of diatoms by a constant mortality coefficient transferring diatoms to fast-sinking detritus and to opal, which is a separate state variable for bookkeeping silicon.

The vertical distribution of the fish state variable is specified according to a 'time allocation vector' derived from the acoustic registrations of the observed DVM pattern (Fig. S4). This time allocation vector accounts for the fraction of time spent at depth during a 24 h cycle by non-migrant as well as migrant organisms. We note that the acoustic observations might reflect organisms other than fish, although we

have no direct evidence of that (Kaartvedt et al. 2019b). The simulated total (surface integrated) fish abundance and growth emerges from feeding on mesozooplankton, metabolic losses (as CO_2, l-DOC, DIP, and fecal particulate matter), and mortality. These processes take place in the entire water column according to the time allocation vector combined with the simulated depth distribution of mesozooplankton. Consequently, to the extent that the simulated mesozooplankton distribute in the mesopelagic zone, they also serve as food for fish, as also indicated by observations (Clarke 1978, Kinzer & Schulz 1985, Bagøien et al. 2001).

The solution to the system of partial differential equations was found numerically, by first doing a semi-discretization of the equations with respect to the depth variable z (discretization of the right-hand side of Eq. 1) and then utilizing a fourth-order embedded Runge-Kutta method for the temporal integration of the semi-discretized equations (Iserles 2009, Butcher 2016, Kennedy & Carpenter 2019). This allowed for variable time steps and local error control. The model code is written in MATLAB® and is available on GitHub (https://zenodo.org/record/8094753).

2.3. Model coefficients

For coefficients that are common to the original MinMod (Table S5), we used, with one exception, the values used by Thingstad et al. (2007, 2021). This exception relates to bacterial growth efficiency (BGE) and their uptake affinity for l-DOC, which in our model also reflects semi-labile DOC. Molar C:P ratios of 250 (corresponding to Y_{BC} = 0.004, Table S5) and 50 in the bacterial diet and bacterial biomass, respectively (Thingstad et al. 2007), suggest a BGE of 20%. This is likely too high for the oligotrophic and warm Red Sea (3–13%, Silva et al. 2019), so we applied a BGE of 5% (i.e. Y_{BC} = 0.001, Table S5) which is closer to Red Sea measurements (Calleja et al. 2018). In previous experimental MinMod studies where glucose was added as l-DOC, the bacterial affinity (α_{BL}) for l-DOC was set to 5.3×10^{-6} and 8×10^{-5} l nmol-P^{-1} h^{-1} at 17°C (Thingstad et al. 2007, 2021). These values consistently caused too efficient C-uptake in bacteria as indicated by far too low simulated l-DOC concentrations, so the affinity was lowered to 1.6×10^{-7} l nmol-P^{-1} h^{-1} (Table S5) in our simulations.

Concerning coefficients that are not part of the original MinMod (Table S5), we applied fixed values (i.e. not temperature dependent) for the light affinities for the 2 autotrophic groups. These values were set as the maximal growth rates (at 27°C) divided by the half-saturation value (200 µmol quanta m^{-2} s^{-1}), of which the latter was adapted from the idealized model of the deep chlorophyll maximum in the oligotrophic ocean by Huisman et al. (2006). Our representation of metabolic losses requires a minimum of 2 coefficients for each organism group. Based on the data compilation of Buitenhuis et al. (2010) and the review by Steinberg & Landry (2017), we used a common parameter set for heterotrophic flagellates, ciliates, and mesozooplankton. For these groups, the respiration (CO_2), detritus (POC), and l-DOC losses amounted to fractions of 0.6 (f_{rHCZ}, Table S5), 0.2 (f_d), and 0.2 (i.e. $1 - f_{rHCZ} - f_d$) of the total loss, respectively. For fishes, the corresponding loss fractions were 0.4, 0.2, and 0.4 (Saba et al. 2021, Liu et al. 2022). There are 4 coefficients associated with detritus. The first 2, i.e. the sinking rates of slow- and fast-sinking detritus, were set 10 and 100 m d^{-1}, respectively (Table S5). These values are the same as in Nowicki et al. (2022) and reflect (on an order of magnitude) measurements made in marine snow-catcher studies (Riley et al. 2012, Giering et al. 2016, Baker et al. 2017). The third coefficient specifies a fragmentation rate of fast-sinking into slow-sinking and further into suspended detritus, and the fourth coefficient is a 'leakage rate' of phosphorus and carbon from suspended detritus to DIP and l-DOC, respectively. These last 2 rates (k_l and k_{frag}, Table S5) were set so that (1) the simulated gravitational flux of the baseline simulation was within the observed variability in the Gulf of Aqaba (Torfstein et al. 2020), and (2) the relative composition of fast-sinking, slow-sinking, and suspended detritus corresponded to that observed in marine snow-catcher experiments (Riley et al. 2012, Baker et al. 2017).

We used a maximum growth rate of fish of 0.054 d^{-1} (Table S5). This value assumes full stomach and use of the digestion time (at 21°C) and growth efficiency reported for *Benthosema pterotum* in the Gulf of Oman assuming a mean fish size of 25 mm (Dalpadado & Gjøsæter 1988). We base the fish affinity (or maximal clearance rate) for mesozooplankton on the allometric relationship for visual predators in Sørnes & Aksnes (2004). This provides a value of order 10^{-6} m^3 s^{-1} (3.6 l h^{-1}) for a 25 mm fish.

2.4. Initialization and forcing of the model

Like Huisman et al. (2006), we initialized the state variables (Table S1) with homogeneous depth distributions (except for fish, see below) and ran the model

with constant forcing (Table S6) until steady state is reached (Figs. S5 & S6). The criterion for steady state is when the absolute differences between the depth-specific concentrations of the state variables at time t and the corresponding concentrations at time $t - 24$ h are less than a predefined tolerance, set here to be 5×10^{-5} nM P.

Temperature affects the biological rates and was specified according to the observed depth profile in Fig. S1B. We used a constant DIP boundary concentration of 1 µmol l^{-1} at 700 m depth, which corresponds to the observation at this depth (Fig. S1F). The silicate concentration was set 10 times higher than the DIP concentrations according to measurements in the Red Sea mesopelagic zone (Wafar et al. 2016). While slow- and fast-sinking detritus (including opal) were lost out of the model domain at 700 m depth, the non-sinking state variables were neither lost nor introduced across this boundary. Conceptually, this means that steady state corresponds to the situation when the net amount of DIP diffusing (according to turbulent diffusivity, Eq. 1) into the model domain equals the amount of phosphorus leaving the model domain by sinking.

Turbulent diffusivity frames the trophic state of the simulated water column by determining the supply of new nutrients and the associated new production (sensu Dugdale & Goering 1967, Eppley & Peterson 1979). For the baseline simulation, this 'bottom-up' forcing was set so that the simulated net primary production (NPP) was in the upper range of the measurements reported between 23 and 28° N in the northern Red Sea (Qurban et al. 2014). These measurements ranged from 9.6 to 79.0 mg C m^{-2} h^{-1}, equivalent to 115–948 mg C m^{-2} d^{-1} assuming a 12 h production cycle. We note that from nitrate uptake experiments, Qurban et al. (2014) estimated turbulent diffusivities about 5 times higher than the value we applied in the baseline (Table 1). Such elevated diffusivity provides NPP higher than 2500 mg C m^{-2} d^{-1} (not shown), which was not observed. As pointed out by Qurban et al. (2014), however, nitrification within the euphotic zone may have been significant in their study, and this might explain the relatively high turbulent diffusivity inferred from their nitrate uptake experiments.

The vertical fish distribution was forced according to the acoustic observations (Fig. S4). Fish mortality rate (all types of mortality) is a closure term of our model and was set at 2 yr^{-1}, which corresponds to the estimate for *B. pterotum* (Svåsand 1983), the common mesopelagic myctophid in the Red Sea (Dalpadado & Gjosaeter 1987, Dypvik & Kaartvedt 2013).

Table 1. Biological carbon pump sensitivity to fish abundance as set by fish mortality rate (δ_F, yr^{-1}). In the No-fish scenario, mesozooplankton is the top predator. Turbulent diffusivity is the same (3×10^{-4} m^2 s^{-1}) in all scenarios. NPP: net primary production; l-DOC: labile dissolved organic carbon; DIP: dissolved inorganic phosphorus; WMDR: weighted mean depth of the mesopelagic community respiration

Quantity	Unit	Scenario			
		High fish abundance $0.5\delta_F$	Baseline $\delta_F = 2$	Low fish abundance $2\delta_F$	No-fish
Fish biomass	g C m^{-2}	2.3	1.4	0.59	0
NPP	mg C m^{-2} d^{-1}	805	920	896	1053
Euphotic depth	m	136	79	32	89
Export at 200 m depth					
Total carbon export	mg C m^{-2} d^{-1}	108	98	129	78
Gravitational	mg C m^{-2} d^{-1}	72	58	40	61
Diffusive (particulate)	mg C m^{-2} d^{-1}	16	6	8	6
Diffusive (l-DOC)	mg C m^{-2} d^{-1}	3	12	62	11
Active	mg C m^{-2} d^{-1}	18	22	18	0
Total phosphorus export	mmol P m^{-2} d^{-1}	0.070	0.050	0.038	0.053
Net upward DIP flux	mmol P m^{-2} d^{-1}	0.070	0.050	0.038	0.053
Gravitational flux attenuation, 200–700 m	m^{-1}	0.00249	0.00233	0.00217	0.00300
Penetration length scale	m	402	429	460	333
Export at 700 m depth					
Gravitational (≈ total)	mg C m^{-2} d^{-1}	20.2	16.9	12.4	13.4
Community respiration and sequestration of carbon below 200 m					
Community respiration	mg C m^{-2} d^{-1}	115	102	135	81
WMDR	m	439	444	413	413
Sequestration proxy	kg C m^{-2}	5.9	5.3	6.5	3.9

2.5. Model sensitivity to top-down and bottom-up forcing

We explored how the simulated microbial food web and the associated carbon export and sequestration respond to variations in the top-down forcing represented by fish mortality and DVM. We halved and doubled the fish mortality relative to the baseline and included a scenario without DVM and consequently zero active flux ('No-fish scenario'). In the latter scenario, like in the original MinMod, mesozooplankton is the top predator and mesozooplankton mortality enters the fast-sinking detritus. We also varied the bottom-up forcing, i.e. the nutrient input to the euphotic zone, as determined by turbulent diffusivity. Relative to the baseline, we tested a halved, a doubled, and a 10-fold increase in the turbulent diffusivity.

2.6. Calculation of active carbon flux and sequestration

The active flux at a certain depth, x, is calculated from the discrepancy between the depth distributions of feeding and metabolic losses of the fish below depth x (Eq. S38). The more their feeding takes place in the epipelagic, the larger the active carbon flux. For example, if simulated zooplankton is mainly distributed in the epipelagic zone, most fish feeding will take place there and the active carbon flux will be higher. The simulated fish losses, however, distribute vertically according to the time spent at depth as given by the acoustical observations. Since fish feeding is also allowed to take place in the mesopelagic zone (to the extent simulated mesozooplankton are present in the mesopelagic zone), part of what is lost in the mesopelagic originates from food ingested in the mesopelagic and is not counted as active flux.

The sequestration time for carbon, i.e. the time for remineralized carbon to circulate back to the ocean surface/atmosphere, increases with the remineralization depth (Boyd et al. 2019). We used the weighted mean depth of the mesopelagic community respiration (WMDR) as a proxy for the efficiency of the mesopelagic carbon sequestration. The deeper this depth, the more efficient is the carbon sequestration. If the community respiration (respiration of all organism groups) between 200 and 700 m amounts to $A = \int_{200}^{700} R(z)\mathrm{d}z + Cflux_{700}$, the WMDR is:

$$\mathrm{WMDR} = \int_{200}^{700} \frac{zR(z) + 700 \times Cflux_{700}}{A}\mathrm{d}z \qquad (2)$$

where $R(z)$ is the depth-specific community respiration. The carbon flux ($Cflux_{700}$) leaving the last depth cell (700 m) is treated here as if it was respired at 700 m depth.

We applied the open-ocean relationship between depth and sequestration time (Fig. 2b in Boyd et al. 2019) to approximate the corresponding sequestration time (in years) for the WMDR. The reported sequestration proxy (with unit kg C m^{-2}) is the product of this sequestration time and the integrated mesopelagic community respiration. We emphasize that this estimate corresponds to the simulated water column being placed in the open ocean rather than in the Red Sea. The water renewal mechanisms and ventilation of the semi-enclosed Red Sea water masses are different from that of the open ocean. The sequestration proxy is therefore not suitable for assessing actual carbon sequestration in the Red Sea but is used here to compare simulated scenarios. Dissolved inorganic carbon (DIC) is not a state variable of the model. Consequently, in the simulations where we varied the turbulent diffusivity, the model did not account for upward mixing of CO_2-enriched water. In nature, this reduces the sequestration of that pool.

3. RESULTS

3.1. Red Sea baseline simulation

The simulated vertical ecosystem structure largely reflects the observed structure (Fig. 2). Simulated DIP (Fig. 2B) and silicate (Fig. 2C) concentrations are depleted in the upper euphotic zone but increase gradually towards the boundary set at 700 m depth. The simulated autotrophs (Fig. 2E) form a deep chlorophyll maximum above the euphotic depth (79 m, Table 1), mesozooplankton abundance (Fig. 2G) increases towards the surface, and the vertical POC flux has a relatively low mesopelagic attenuation, as also reflected by the observations (Fig. 2H). The simulated distribution of l-DOC (Fig. 2D), however, shows a subsurface maximum contrasting with the observed DOC maximum at the surface (discussed in Section 4.5).

The simulated fish ingestion decreases rapidly with depth (Fig. 3A) reflecting the simulated food source (mesozooplankton, Fig. 2G). The metabolic losses of the fishes (excretion, respiration, defecation, and mortality), however, are more evenly distributed in the water column but with a maximum at their mesopelagic daytime depth as well as at their epipelagic nighttime depth (Fig. 3A). This pattern is

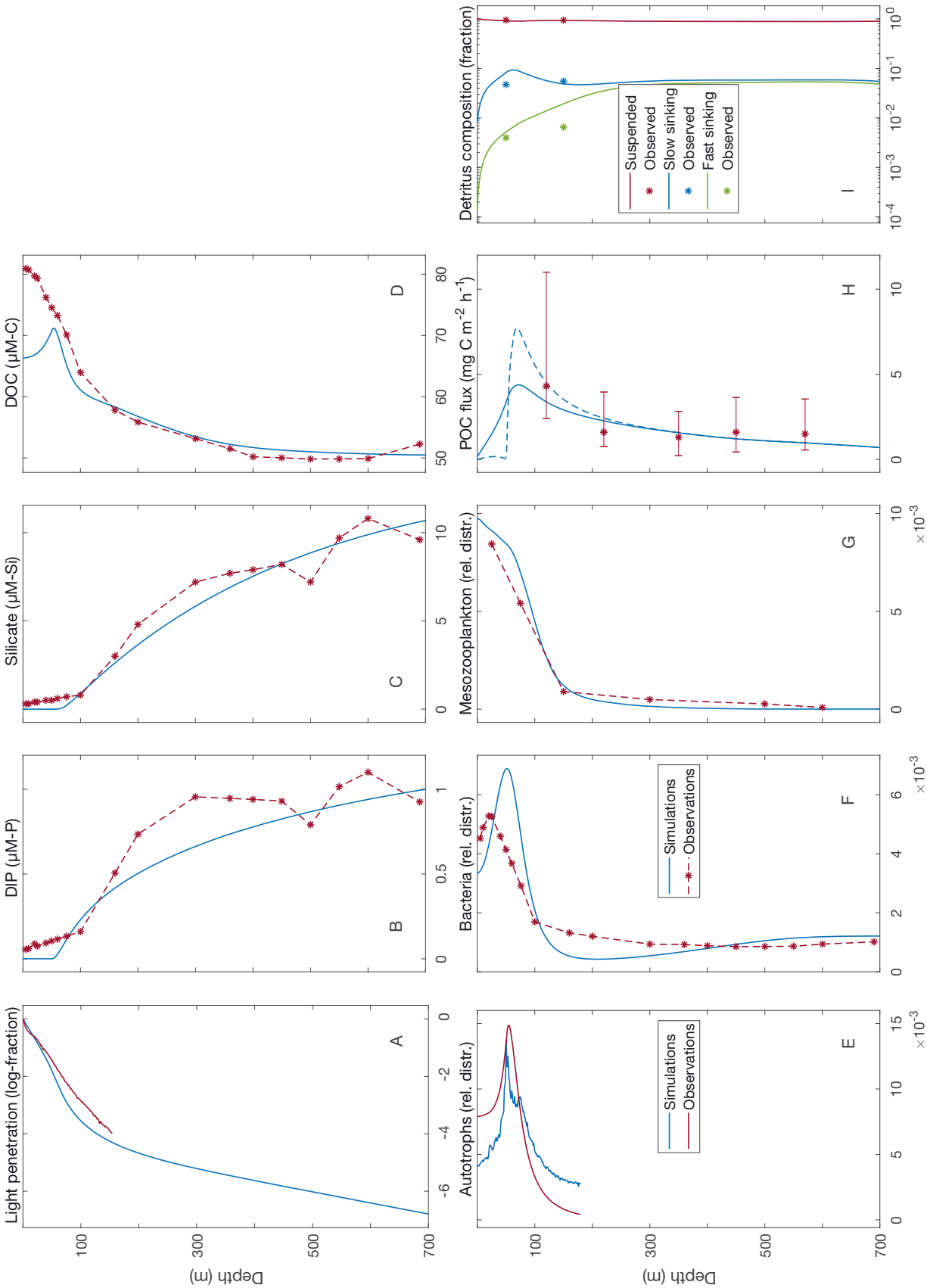

Fig. 2. Simulated baseline scenario and observed depth profiles. (A,B,D–G) Observations in these panels are the average of the measurements from the Red Sea that are shown in Fig. S1. (C) Silicate is based on the dissolved inorganic phosphorus (DIP) distributions adjusted with the Si:DIP ratio from the Red Sea in Wafar et al. (2016). In (D), the simulated dissolved organic carbon (DOC) concentration is the sum of the labile DOC (l-DOC) concentration provided by the model and a background concentration of recalcitrant DOC assumed to be 50 μM at all depths. (H) The particulate organic carbon (POC) flux represents observations from sediment traps placed at average depths of 123, 225, 346, 462, and 576 m in the Gulf of Aqaba in the period July to October in 2014 and 2015 (Torfstein et al. 2020). The solid and the broken line are the simulated gravity flux and the sum of the gravity and diffusive POC fluxes, respectively. (I) The simulated detritus compositions (solid lines) are shown together with the relative compositions at 50 m depth at the Porcupine Abyssal Plain site (Riley et al. 2012)

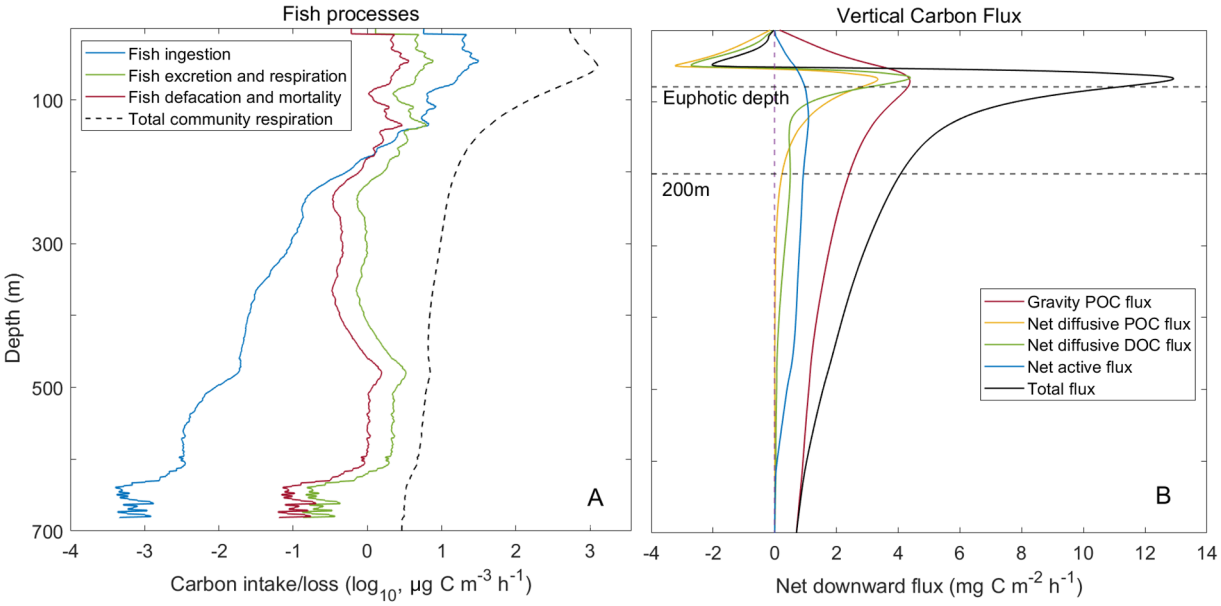

Fig. 3. (A) Fish processes and total community metabolism and (B) vertical carbon flux as a function of depth in the baseline scenario. Negative values of vertical carbon flux mean that the net flux is upward. The gravity flux is the sinking of slow- and fast-sinking detritus (dead particulate organic carbon, POC). Diffusive POC flux is the diffusive flux of suspended detritus (dead POC) and of microbial organisms (living POC). Active flux is the migrant carbon transport calculated according to Eq. (S38)

largely determined by time spent at depth as given by the acoustic observations (Fig. S4). Between 480 and 600 m depth, the simulated fish losses of CO_2 and l-DOC (subsequently respired by bacteria) make up a relatively large fraction (up to ~50 %) of the simulated community respiration (Fig. 3A). This high contribution of fish to the community respiration accords with the existence of fish-mediated heterotrophic activity at the mesopelagic daytime depth of these fishes (Calleja et al. 2018, Morán et al. 2022).

According to expectations for the Red Sea and more generally for the oligotrophic subtropical ocean (Malviya et al. 2016), the baseline simulation shows relatively low presence of diatoms relative to the non-diatom autotrophs (Fig. S6). This is particularly true for the upper 50 m where diatoms contribute to less than 1 and 7 % of the NPP and the autotrophic biomass, respectively (not shown). At the bottom of the euphotic zone (79 m), however, modeled diatoms are more influential and make up almost 50 % of the NPP. These diatoms consume the upward-diffusing silicate and cause silicate depletion towards the surface (Fig. 2C), as also observed for the Red Sea (Wafar et al. 2016).

3.2. Contribution of fish DVM to the BCP

In the baseline scenario, the total community respiration below 200 m depth is 102 mg C m^{-2} d^{-1} (Table 1), and the corresponding WMDR is 444 m (Table 1). For the open ocean, this depth corresponds to ~150 yr of sequestration time (Fig. 2b in Boyd et al. 2019). If this is taken as the average sequestration time for the carbon respired below 200 m, our proxy (see Section 2.6) for carbon sequestration is 5.3 kg C m^{-2} in the baseline scenario compared to 3.9 kg C m^{-2} in the No-fish scenario (Table 1). Thus, the introduction of fish DVM to the model increases carbon sequestration by 36 %. Two mechanisms are responsible for this enhanced carbon sequestration by fish in our model: (1) active carbon flux attenuates less than the passive (i.e. gravitational and diffusive) fluxes above ~500 m depth (Fig. 3B), and (2) migrators fuel the gravitational flux deep into the mesopelagic zone.

3.2.1. Active flux attenuates less than passive flux

Due to a higher depth penetration (i.e. lower attenuation) of the active carbon flux in comparison with the gravitational and diffusive fluxes, the relative importance of the active flux increases with increasing depth (Fig. 4). At 200 m depth, the contribution of the active flux amounts to 22 % but increases to 32 % in the depth range 410–450 m. Below this depth range, the relative contribution of the active carbon flux decreases until ceasing at the bottom of the DVM zone, where the gravitational flux amounts to ~100 % of the total carbon flux (Fig. 4).

3.2.2. Fueling of the gravitational carbon flux

Although active flux ceases below the DVM zone, fish DVM makes a notable footprint on the carbon flux also at depths below the DVM zone. This is due to fueling of the gravitational flux by fish defecation and mortality within the DVM zone (red line in Fig. 3A). This transfer of carbon from the active to the gravitational flux reduces the attenuation of the gravitational flux throughout the DVM zone (Fig. 3B). Compared to the No-fish scenario (i.e. without active flux), the fish-mediated fueling reduces the attenuation coefficient of the gravitational flux by 22%, i.e. from 0.30 × 10^{-3} m^{-1} in the No-fish scenario to 0.23 × 10^{-3} m^{-1} in the baseline scenario (Table 1). This reduced attenuation corresponds to an increase in the depth penetration of the gravitational carbon flux by around 100 m (from 333 to 429 m, Table 1).

3.3. Fish associated top-down effects

Fish mortality is the closure term of our food-web model. Adjustment of this term causes pronounced top-down cascade effects on the food web (Figs. 5 & 6) that propagate to carbon export and sequestration (Table 1, Fig. 7). Halving of the fish mortality leads to a 58% increase in the steady-state fish abundance (relative to that of the baseline scenario, Table 1). Below, we refer to this simulation as the 'high fish abundance' scenario. Doubling of the fish mortality leads to a 64% decrease in fish abundance, and we refer to this simulation as the 'low fish abundance' scenario.

3.3.1. High fish abundance scenario

Compared with the baseline, the high fish abundance scenario (halving of the fish mortality rate) provides reduced mesozooplankton abundance, which causes increased abundances of ciliates, bacteria, and diatoms (Fig. 5). Despite a slight reduction in the NPP, carbon export at 200 m depth increases relative to the baseline (Table 1). It might appear surprising that the increased carbon export is not caused by increased active flux but rather by increased gravitational flux (from 58 to 72 mg C m^{-2} d^{-1}, Table 1). Fish feeding and subsequent metabolic processes depend on the product of fishes and mesozooplankton abundances. Since the food-web cascade involves reduced mesozooplankton abundance and consequently less fish feeding, the net effect is a lower active flux in the high

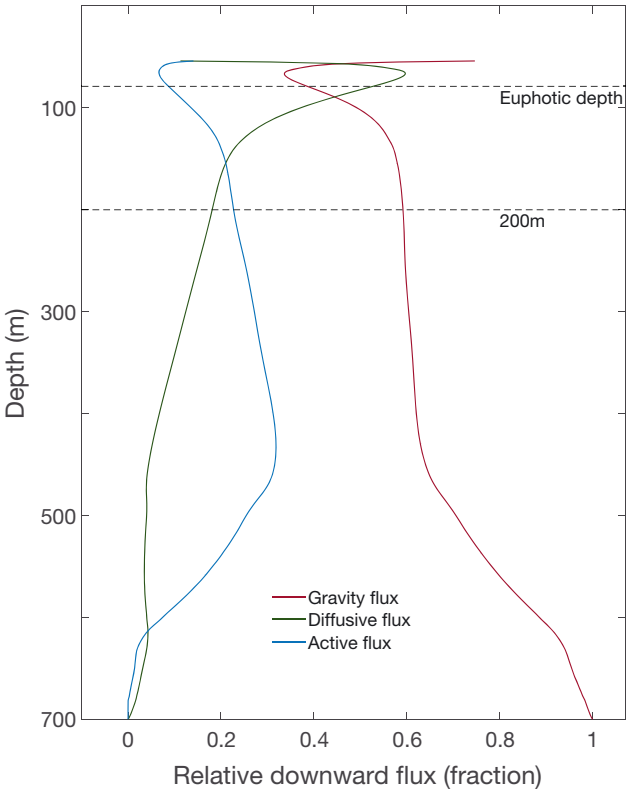

Fig. 4. Relative contribution of the gravitational, diffusive, and active fluxes to the total downward carbon flux as a function of depth in the baseline scenario. Above 54 m, relative contributions are not plotted, as the total and the net diffusive fluxes are upward (see Fig. 3B)

fish abundance scenario (18 mg C m^{-2} d^{-1}, Table 1) than in the baseline scenario (22 mg C m^{-2} d^{-1}).

The larger gravitational flux in the high fish abundance scenario than in the baseline scenario is partly caused by a deepening of the euphotic zone from 79 to 136 m depth (Table 1). This deepening of the euphotic zone involves a shift from non-diatom autotrophs to diatoms (Fig. 5) and an associated diatom 'nutrient trap' at the bottom of the euphotic zone. Here, diatoms trap new DIP, in addition to silicate, resulting in reduced diffusive flux of new DIP into the upper euphotic zone (see Section 4).

3.3.2. Low fish abundance scenario

In the low fish abundance scenario, the food-web cascade is opposite to that of the high fish abundance scenario (Figs. 5 & 6). Elevated mesozooplankton biomass in the low fish abundance scenario (red line in Fig. 6C) results in fewer ciliates (Fig. 6B) and bacteria (Fig. 6D), and a strong dominance of non-

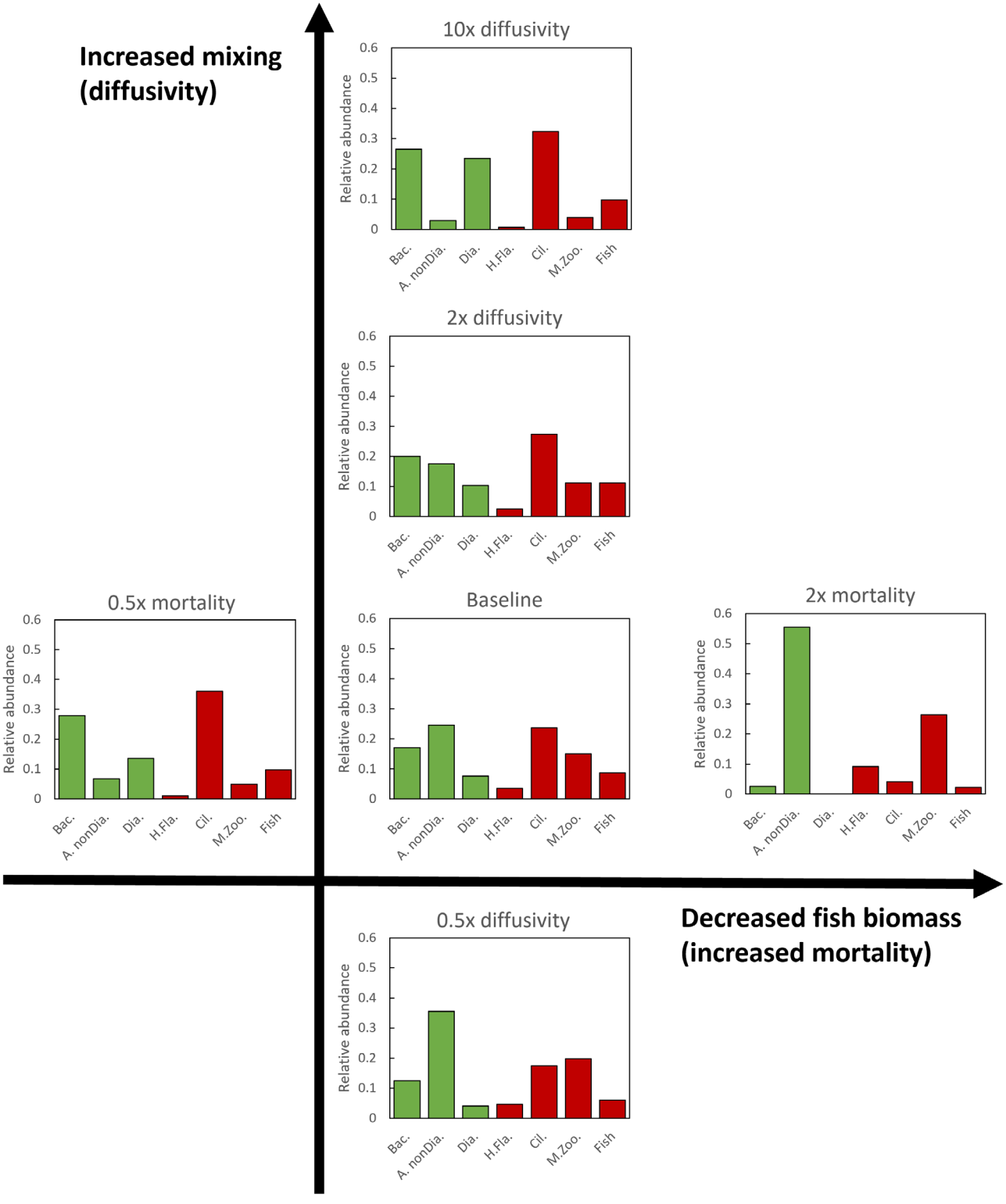

Fig. 5. Food-web composition for different fish abundances (fish mortality rate) and water column mixing (turbulent diffusivity). The *y*-axis of each histogram shows the relative abundance of each organism group (fraction of total biomass). The fish mortality rate (δ_F) and turbulent diffusivity (κ) of the baseline scenario are 2 yr^{-1} and 3×10^{-4} m^{-2} s^{-1}, respectively

diatom autotrophs (Fig. 6E). Absence of diatoms (Fig. 6F) leads to a euphotic zone replenished with silicate (Fig. 6I). Along with this cascade is a pronounced shoaling of the euphotic zone to 32 m depth (Table 1, Fig. 7B) and an associated shoaling of the DIP nutricline (Fig. 6H). Consequently, primary pro-

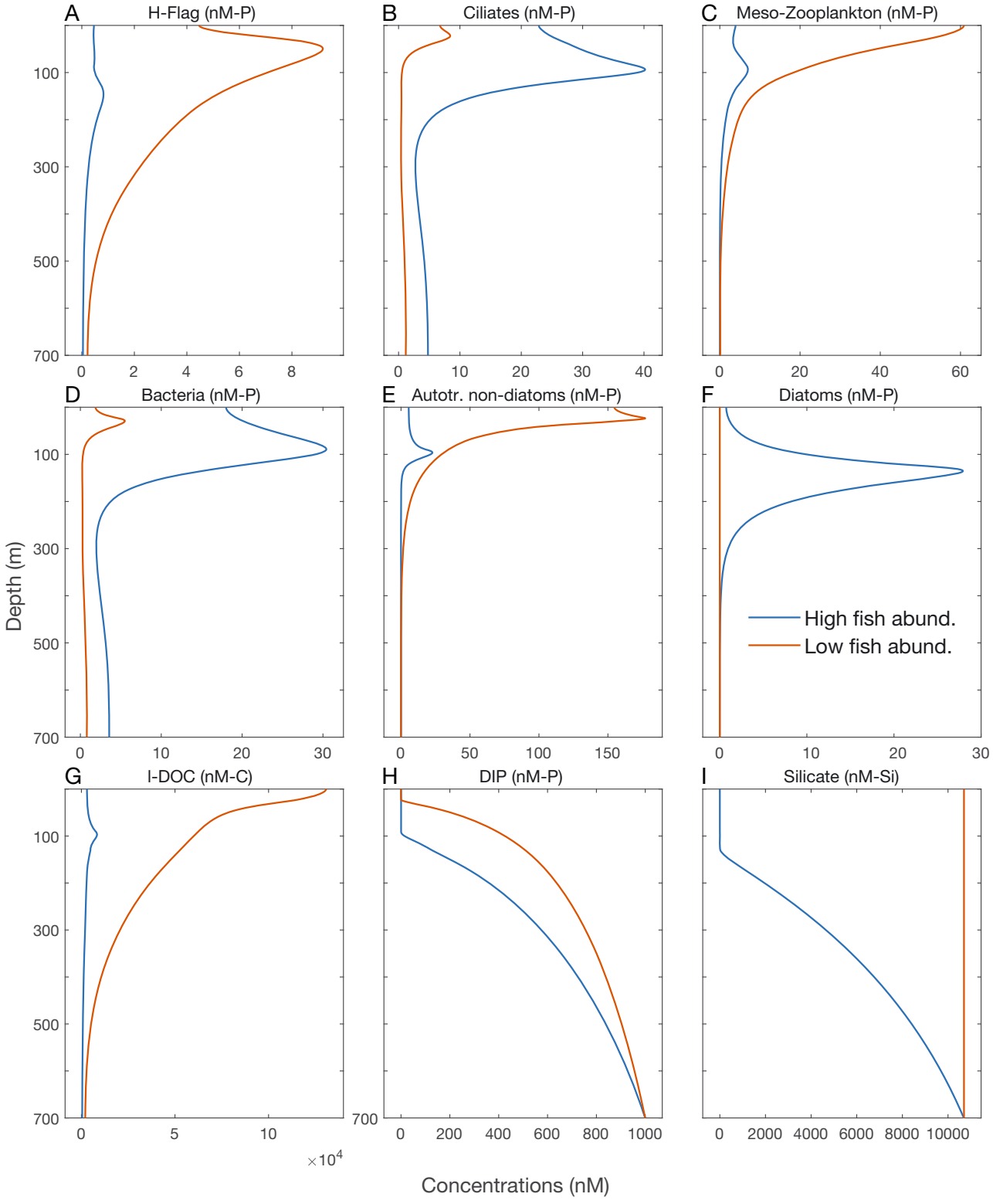

Fig. 6. Depth profiles of organisms and nutrients for the high (red) and low (blue) fish abundance scenarios. High fish abundance causes a food-web cascade involving a strong diatom nutrient trap and deep euphotic zone (136 m, Table 1). Low fish abundance causes a food web cascade involving elimination of diatoms, replete silicate throughout the water column, and a shallow euphotic zone (32 m, Table 1). The fish mortality rates were half and double the baseline mortality in the high and low fish abundance scenarios, respectively

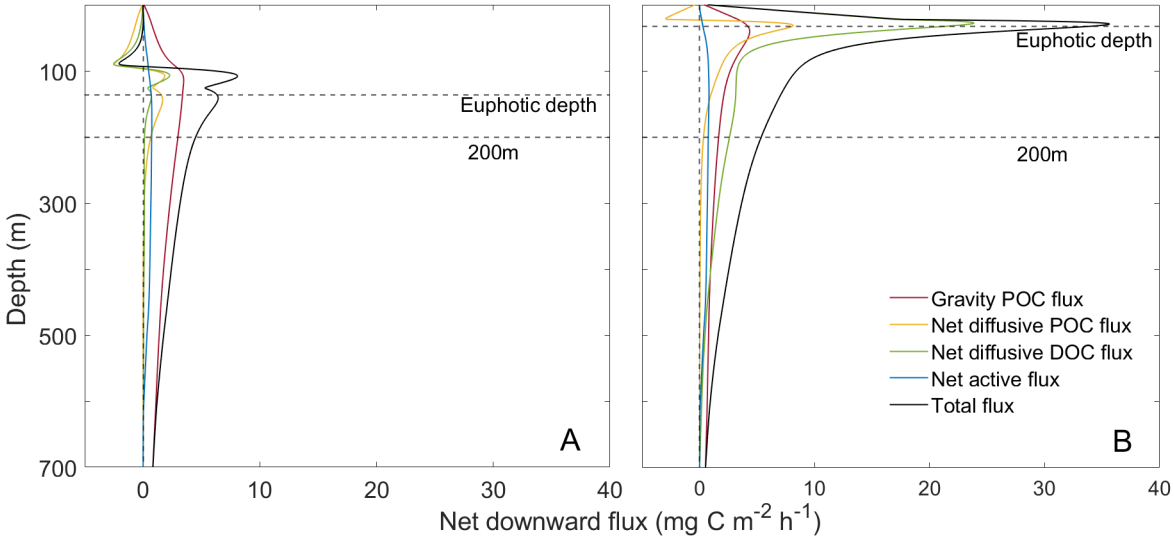

Fig. 7. Depth profiles of carbon export in the (A) high and (B) low fish abundance scenarios. The fish mortality rates were half and double the baseline mortality in the high and low fish abundance scenarios, respectively

duction occurs much shallower in the low fish abundance scenario than in the high fish abundance scenario. This implies a longer epipelagic sinking distance and thereby greater attenuation of the gravitational flux before it reaches the mesopelagic zone (Table 1, Fig. 7B). Furthermore, the total dominance of non-diatom autotrophs, i.e. absence of diatoms, results in a reduced *f*-ratio and larger influence of non-sinking and slow-sinking detritus than in the scenarios where diatoms are present. In sum, this leads to a much lower gravitational flux, nearly half of that in the high fish abundance scenario (Table 1, Fig. 7). On the other hand, the reduced influence of bacteria in the low fish abundance scenario (red line in Fig. 6D) causes a build-up of l-DOC in the epipelagic zone (red line in Fig. 6G), leading to increased diffusive flux of l-DOC out of the epipelagic and into the mesopelagic zone (Table 1, Fig. 7).

3.4. Nutrient-associated bottom-up effects

The supply of new nutrients into the euphotic zone is determined by the turbulent diffusivity in our model. Not surprisingly, this supply greatly affects the magnitude of the NPP (Table 2). Halving and doubling of the turbulent diffusivity cause a 45% reduction and a 77% increase in the baseline NPP, respectively (Table 2). Unlike the top-down effect from fish abundance, the carbon export and sequestration tightly follow the NPP for this 4-fold variation in diffusivity (Table 1). At the highest diffusivity level (10 times the baseline), however, carbon export increases (6.3-fold) much more than the NPP (4.2-fold). This is due to increased new production relative to regenerated production (i.e. increased *f*-ratio) involving increased diatom dominance (Fig. 5). Like increased fish abundance, increased turbulent diffusivity stimulates diatoms at the expense of the non-diatom autotrophs, albeit with one notable difference. While increased fish biomass induces diatom dominance along with a deepening of the euphotic zone (Table 1, Fig. 7), increased turbulent diffusivity induces diatom dominance along with a shoaling of the euphotic zone (Table 2).

4. DISCUSSION

4.1. Effects of mesopelagic fishes on Red Sea carbon flux

Our results agree with the expectation that mesopelagic fishes are important for carbon export in the Red Sea. In our baseline scenario, the active carbon flux by fish amounted to 32% of the total carbon flux at 440 m depth (Fig. 4). Between 480 and 600 m depth, which corresponds to the daytime depth of the fishes, our results suggest that the migrating fishes are responsible for a large fraction of the community metabolism (Fig. 3A). This supports previous evidence that fish losses fuel a prokaryotic hotspot in this mesopelagic depth interval (Calleja et al. 2018, Morán et al. 2022). Comparison of the scenarios with (baseline) and without (No-fish) active flux suggests that the fish DVM increased carbon sequestration by 36% (Table 1).

Table 2. Biological carbon pump sensitivity to water column mixing as set by turbulent diffusivity (κ, $m^2\ s^{-1}$). Fish mortality rate is the same in all scenarios ($2\ yr^{-1}$). The baseline is identical to that in Table 1; other abbreviations as in Table 1

Quantity	Unit	Scenario			
		Low mixing 0.5κ	Baseline $\kappa = 3\times10^{-4}$	High mixing 2κ	Very high mixing 10κ
Fish biomass	g C m^{-2}	0.74	1.4	2.4	6.3
NPP	mg C m^{-2} d^{-1}	502	920	1631	3866
Euphotic depth	m	92	79	65	40
Export at 200 m depth					
Total carbon export	mg C m^{-2} d^{-1}	55	98	176	622
Gravitational	mg C m^{-2} d^{-1}	32	58	101	311
Diffusive (particulate)	mg C m^{-2} d^{-1}	3	6	17	215
Diffusive (l-DOC)	mg C m^{-2} d^{-1}	8	12	18	3
Active	mg C m^{-2} d^{-1}	12	22	40	93
Total phosphorus export	mmol P m^{-2} d^{-1}	0.028	0.050	0.092	0.427
Net upward DIP flux	mmol P m^{-2} d^{-1}	0.028	0.050	0.092	0.427
Gravitational flux attenuation, 200–700 m	m^{-1}	0.00236	0.00233	0.00230	0.00215
Penetration length scale	m	424	429	435	465
Export at 700 m depth					
Gravitational (≈ total)	mg C m^{-2} d^{-1}	9.2	16.9	30.1	104.0
Community respiration and sequestration of carbon below 200 m					
Community respiration	mg C m^{-2} d^{-1}	58	102	184	666
WMDR	m	439	444	443	440
Sequestration proxy	kg C m^{-2}	3.0	5.3	9.5	34.3

From a synthesis of existing information on fecal pellet sinking and active migratory flux of fish, Saba et al. (2021) estimated that fish contribute an average of 16.1 ± 13% to total carbon flux out of the euphotic zone. The contribution to carbon sequestration also depends on the depth penetration of the active versus the passive flux further down in the mesopelagic zone. As illustrated by Saba et al. (2021), carbon being exported to depths of 100, 400, and 1000 m in the open ocean correspond to sequestration times of 14, 104, and 352 yr, respectively. When active flux is less attenuated with depth than the gravitational flux (such as above 450 m depth in Fig. 3B), active flux contributes to deeper and thereby higher carbon sequestration. In the northeast Pacific, Davison et al. (2013) found a contribution of fish mediated export of 15–17% out of the epipelagic zone. At 400 m depth, however, they found that the contribution of active flux increased to approximately 50%. Such increased contribution of active flux with increased depth is also reflected in our study, although to a lesser extent than in Davison et al. (2013). The maximal contribution of the active flux in our baseline study is 32% at around 430 m (Fig. 4).

As noted in Section 1, it is reasonable to expect that mesopelagic fishes are important in Red Sea carbon export. All fishes take part in DVM (Klevjer et al. 2012, Dypvik & Kaartvedt 2013), and mesozooplankton migration appears limited (Weikert 1982, Dypvik & Kaartvedt 2013). Another factor affecting export is the high temperature in the entire water column (>21°C, Fig. S1B), which might cause elevated remineralization rates and high attenuation of the passive flux (Marsay et al. 2015, Mazuecos et al. 2015, Robinson 2019). Accordingly, Kheireddine et al. (2020) considered high temperature a likely cause for the rapid remineralization and the high flux attenuation of POC that they found just below the productive layer in the Red Sea. Below 200 m depth, however, a low POC flux attenuation was indicated in their study as well as in a study by Torfstein et al. (2020). Our baseline scenario agrees with this observed pattern involving a high POC flux attenuation between 100 and 200 m depth and a low attenuation in the mesopelagic zone (Figs. 2H & 3B).

In the mesopelagic zone, our results suggest that fueling of the gravitational flux by the migrators contributes to a lowering of the POC flux attenuation. In principle, mesopelagic fueling of the gravitational flux by migrators might cause negative attenuation for certain situations and depth intervals. Such negative attenuation is indeed indicated by the somewhat higher POC flux at 570 than at 350 m depth in the Gulf of Aqaba (Table 3 in Torfstein et al. 2020). More

generally, our results suggest that DVM fueling of the gravitational flux in the mesopelagic zone has important implications for the interpretation of flux attenuation coefficients and Martin curves derived from sediment trap observations (Buesseler & Boyd 2009, Marsay et al. 2015, Buesseler et al. 2020). We expect that spatial and temporal variation in these coefficients should reflect not only degradation processes but also fueling by DVM organisms.

We note that the active carbon flux might have been underestimated in our model. This is because we have assumed that metabolic losses and feeding by fish are in proportion to the time spent at depth as given by the acoustical observations. For example, the role of active flux would have been larger if we had restricted feeding to occur close to the surface and assumed that metabolic losses (such as defecation) largely took place at the mesopelagic daytime depth of the fish. According to the acoustical observations, the fish spend close to 50% of their time in the epipelagic zone. Thus, in our model, a substantial part of their defecation and mortality enters the gravitational flux in the epipelagic zone (Fig. 3A) and is therefore not bookkept as mesopelagic active carbon flux in our simulations.

4.2. Red Sea — representative of the oligotrophic subtropical ocean?

Using a global steady-state data-assimilated model, Nowicki et al. (2022) found that the biome represented by the subtropical gyres had the lowest carbon sequestration in the ocean, amounting to 2.2 kg C m^{-2}. Closest to this estimate is our scenario (3.0 kg C m^{-2}, Table 2) with a turbulent diffusivity half of that in the baseline scenario. One notable difference between our scenario and Nowicki et al. (2022) is that the active flux of their model (termed 'migrant pump export' in their study) is near zero in oligotrophic subtropical waters. This is because their migrant pump was largely driven by mesozooplankton that, like in the Red Sea, were assumed to have little or no DVM in the oligotrophic subtropical waters. We note, however, that the carbon sequestration in the model of Nowicki et al. (2022) was constrained by their oxygen budget of the interior ocean. This means that explicit inclusion of fish DVM in their model would not affect total carbon sequestration but would likely increase the importance of active, at the expense of passive, carbon flux. Like the Red Sea, large daily acoustical migration patterns are found in the transparent subtropical ocean (Bianchi & Mislan 2016, Klevjer et al. 2016, Aksnes et al. 2017, Kaartvedt et al. 2019a). Thus, increased awareness of the role of active flux in these waters seems warranted. As noted above, however, a further major difference between the Red Sea and the subtropical ocean is the high temperature in the Red Sea mesopelagic zone which might imply shallower POC and DOC remineralization in the Red Sea than in the subtropical ocean.

4.3. Potential top-down effects of mesopelagic fishes

4.3.1. Cascading effects on the microbial food web

Since the first attempts to model vertical structure and primary production (e.g. Radach & Maier-Reimer 1975), it has been known that vertical mixing is of first order in framing the NPP of ecosystem models. This is central in models predicting decline in oceanic primary production and carbon export because of global warming and associated increase in density stratification (Sarmiento et al. 1998, 2004, Bopp et al. 2001). Our model is no exception to this and underlines the crucial bottom-up control vertical mixing has in determining the trophic state and the associated carbon export in a water column (Table 2). A more important insight from our study, however, is how zooplanktivorous predators modulate carbon export through cascading effects on the microbial food web. Although uncertain to what degree such cascades are present in nature, they are obviously important in modeling (Getzlaff & Oschlies 2017) and consequently for the realism and interpretation of forecast studies involving ecosystem and biogeochemical models. Our model does not represent prokaryotic phytoplankton (i.e. pico-phytoplankton) as a separate state variable. Although their photosynthesis is assumed to be included in the non-diatom autotrophs, they are not represented as a separate food source for the heterotrophic flagellates (Fig. 1). This omission likely affects the sensitivity of the model to trophic cascades.

Cascading top-down effects from changes in predator abundance can be significant in nature but hard to observe and more seldom demonstrated in the open ocean than in terrestrial, freshwater, and benthic systems (Baum & Worm 2009). The kernel of our model, MinMod, has been developed in close association with observations from mesocosm experiments that do provide evidence of trophic cascades from mesozooplankton (i.e. copepods) on the microbial food web (Thingstad 2020 and references therein). According to observational and theoretical expec-

tations (Wollrab & Diehl 2015, Thingstad 2020), increased predation pressure from fishes on mesozooplankton result in cascades that, in our depth-resolved model, propagate into relatively large variations in the gravitational and diffusive fluxes (Table 1, Fig. 6).

In the high fish abundance scenario, the gravitational carbon export (72 mg C m^{-2} d^{-1}, Table 1) out of the epipelagic zone is much higher than the DOC export (3 mg C m^{-2} d^{-1}). This is reversed in the low fish abundance scenario, where the DOC export (62 mg C m^{-2} d^{-1}) is higher than the gravitational export (40 mg C m^{-2} d^{-1}). Such an increase in diffusive DOC export accords qualitatively with expectations in previous studies (Thingstad et al. 1997, Thingstad & Rassoulzadegan 1999): decreased fish biomass causes a shift towards more mesozooplankton, fewer ciliates, and more heterotrophic flagellates. This increases the predation on bacteria, reduces the l-DOC consumption, and l-DOC accumulates in the euphotic zone, which in turn leads to increased diffusive DOC transport out of the epipelagic zone.

4.3.2. Top-down effects on the depth of the euphotic zone

Top-down cascading effects from fishes and zooplankton on water clarity and consequently on the euphotic depth are well known from limnetic studies (Mazumder et al. 1990, Sarnelle 1993, Vanni et al. 1997) but to our knowledge not in oceanography. The fish-mediated food-web cascade that changes the euphotic depth in our model relates to the competition between diatoms and non-diatom autotrophs in the model. Because diatoms have a high maximal growth in our model (Table S5; Thingstad et al. 2007, see also Furnas 1990, Egge & Aksnes 1992), although with a low affinity for DIP relative to the non-diatom autotrophs, they can, under certain conditions, compete with the non-diatoms. Diatoms, however, require silicate, and in our baseline scenario this leads to silicate depletion and thereby limited diatom growth in the upper euphotic zone. The non-diatom autotrophs do not depend on silicate and benefit from a higher growth affinity than diatoms for DIP, which is more rapidly remineralized within the euphotic zone. Under these circumstances, diatoms establish at the bottom of the euphotic zone where they trap new silicate and DIP that are continuously supplied from below by turbulent diffusivity.

4.4. Diatom nutrient trap

The diatom nutrient trap is an emergent property of our depth-resolved MinMod that might account for the observational evidence that diatoms appear able to grow and dominate the deep chlorophyll maximum of stratified oligotrophic water columns (Crombet et al. 2011, Latasa et al. 2017, Tréguer et al. 2018). According to our model, diatoms trap new DIP, in addition to silicate, at the bottom of the euphotic zone. This trapping causes reduced diffusive nutrient transport to the autotrophs in the shallower part of the euphotic zone with reduced self-shading and deepening of the euphotic zone as a consequence. This nutrient trap is strengthened by diatoms sinking. Such sinking drains the euphotic zone of DIP, as also observed in enclosure experiments (Wassmann et al. 1996).

In our high fish abundance scenario, decreased grazing from mesozooplankton on diatoms makes the diatom nutrient trap stronger and the euphotic zone deeper than in the baseline scenario (Table 1). The opposite effect is seen in the low fish abundance scenario: diatoms are outcompeted, and silicate becomes replete throughout the entire water column (Fig. 6I). Without the trapping of upward-diffusing DIP (and silicate) by diatoms in this scenario, the abundance of non-diatom autotrophs increases, their light absorption increases, and the euphotic zone shoals accordingly (Table 1, Fig. 7).

We summarize 3 (related) mechanisms that underly the increased gravitational flux in the high fish abundance scenario. First, with a deep euphotic zone, primary production (particularly the new production) is located closer to the mesopelagic zone. For sinking particles, this means a shorter distance to travel from the epi- to the mesopelagic zone. Second, the increased diatom dominance increases new, relative to regenerated, production (increased *f*-ratio). Third, the change from non-diatom autotrophs to diatoms implies increased influence of opal and fast-sinking, relative to slow-sinking, detritus, which increases the depth penetration of the gravitational flux.

4.5. Limitations and future research

A challenge in predicting migrant carbon flux by fish is the lack of a mechanistic foundation for behavioral modeling that enables realistic spatial positioning of fish in the water column as a function of time. If behavioral mechanisms are to be assumed for the mesozooplankton as well as for their predators, this

becomes even more challenging as it involves predator–prey games (e.g. Pinti et al. 2021). We avoided behavioral modeling by using acoustic observations to force the depth distribution of the DVM organisms (as well as those organisms not undertaking DVM). This approach is facilitated by the apparent lack of mesozooplankton DVM in the Red Sea but is inadequate for systems involving mesozooplankton migration and associated predator–prey games. In our Red Sea application, it is the time spent at depth over a 24 h cycle, and not the migration per se, that affects the depth distributions of fish feeding, metabolism, mortality, and the resulting active carbon flux. This implicit way of representing fish has 2 advantages. First, it does not require uncertain assumptions of behavioral characteristics such as swimming speed, timing of migration, migration amplitude, and the proportion of individuals that migrate. Second, it does not require hourly or higher temporal model resolution to accurately mimic time spent at different depths, which might be advantageous in time-demanding global models (e.g. Aumont et al. 2018, Nowicki et al. 2022).

A limitation, however, is that the forced depth distribution of fishes is the same for all of our scenarios. Since the discovery of the deep sound-scattering layers, it has been known that light is a proximate control for DVM (reviewed by Kaartvedt et al. 2019a). This is utilized in models using simple behavioral rules relating the depth of a migrant organism to light (Bianchi et al. 2013, Aumont et al. 2018, Nowicki et al. 2022) but does not solve the challenge associated with many, often overlapping, organism layers including migrators as well as non-migrators. Thus, forcing DVM with acoustic observations might also be an alternative in global studies. The need for extensive global acoustic coverage might be reduced by utilization of the empirical evidence that, across very different oceanographic conditions, the depth distributions of acoustic backscatter become more similar when expressed as a function of optical instead of absolute depth (Røstad et al. 2016a,b, Aksnes et al. 2017).

The top-down cascading effects in our model, like in all ecosystem models, are controlled by the unavoidable and sometimes hidden 'closure term' (Mitra 2009), i.e. the term that defines the loss rate(s) of the top-predator(s) in the model. Using a NPZD (nutrient, phytoplankton, zooplankton, detritus) model in combination with a global biogeochemistry circulation model, Getzlaff & Oschlies (2017) warned that the closure term, represented by zooplankton mortality rate in their study, should be treated carefully. In their model, relatively small variations in this rate caused important and sometimes counterintuitive responses in the simulated lower trophic levels and in the simulated biogeochemistry. The caution made by Getzlaff & Oschlies (2017) also applies to our study, where fish mortality rate is a closure term. This means that our result on how the diatom nutrient trap weakens and the euphotic depth shallows with increased fish mortality rate, e.g. by fishing, serves at best as a hypothesis for how nature might work and not as evidence for how fishing on planktivores affects the euphotic depth.

There are discrepancies between our Red Sea baseline simulation and observations that could have been minimized by adjusting the model's coefficient values. Such calibration (or tuning) is sometimes incorrectly referred to as validation and offers numerous ways to fit simulations to observations although at a high risk of hiding errors with other errors. We emphasize one notable discrepancy in our study that did involve tuning (see Section 2.3). In the baseline scenario, the observed DOC maximum is at the surface while the baseline simulation provides a subsurface maximum (Fig. 2D). There are several ways to reduce this discrepancy, e.g. by adjusting the fish mortality (see Fig. 6G), the bacterial affinity for l-DOC, and/or assuming photosynthetic carbon overflow linked to light intensity (Cherrier et al. 2015, Roshan & DeVries 2017) rather than to autotrophic net growth as in our model. There is little doubt that characterization of DOC lability and DOC production involving photosynthetic overflow deserve future attention. Roshan & DeVries (2017) found that DOC production and export display a pronounced peak in the oligotrophic subtropical ocean, and that this production might help to explain, at least in part, the perceived imbalance between autotrophy and heterotrophy in the open ocean (del Giorgio & Duarte 2002).

Acknowledgements. This study received funding from the European Union's Horizon 2020 under grant agreement no. 817806 ('Sustainable management of mesopelagic resources', SUMMER) and under grant agreement no. 326896 from the Norwegian Research Council ('How can fisheries contribute to a sustainable future?').

LITERATURE CITED

Aksnes DL, Røstad A, Kaartvedt S, Martinez U, Duarte CM, Irigoien X (2017) Light penetration structures the deep acoustic scattering layers in the global ocean. Sci Adv 3: e1602468

Aumont O, Maury O, Lefort S, Bopp L (2018) Evaluating the potential impacts of the diurnal vertical migration by

marine organisms on marine biogeochemistry. Global Biogeochem Cycles 32:1622–1643
Bagøien E, Kaartvedt S, Aksnes DL, Eiane K (2001) Vertical distribution and mortality of overwintering *Calanus*. Limnol Oceanogr 46:1494–1510
Baker CA, Henson SA, Cavan EL, Giering SLC and others (2017) Slow-sinking particulate organic carbon in the Atlantic Ocean: magnitude, flux, and potential controls. Global Biogeochem Cycles 31:1051–1065
Baum JK, Worm B (2009) Cascading top-down effects of changing oceanic predator abundances. J Anim Ecol 78: 699–714
Belcher A, Saunders RA, Tarling GA (2019) Respiration rates and active carbon flux of mesopelagic fishes (Family Myctophidae) in the Scotia Sea, Southern Ocean. Mar Ecol Prog Ser 610:149–162
Bianchi D, Mislan KAS (2016) Global patterns of diel vertical migration times and velocities from acoustic data. Limnol Oceanogr 61:353–364
Bianchi D, Stock C, Galbraith ED, Sarmiento JL (2013) Diel vertical migration: ecological controls and impacts on the biological pump in a one-dimensional ocean model. Global Biogeochem Cycles 27:478–491
Bianchi D, Carozza DA, Galbraith ED, Guiet J, DeVries T (2021) Estimating global biomass and biogeochemical cycling of marine fish with and without fishing. Sci Adv 7:eabd7554
Bopp L, Monfray P, Aumont O, Dufresne JL and others (2001) Potential impact of climate change on marine export production. Global Biogeochem Cycles 15: 81–99
Boyd PW, Claustre H, Levy M, Siegel DA, Weber T (2019) Multi-faceted particle pumps drive carbon sequestration in the ocean. Nature 568:327–335
Buesseler KO, Boyd PW (2009) Shedding light on processes that control particle export and flux attenuation in the twilight zone of the open ocean. Limnol Oceanogr 54: 1210–1232
Buesseler KO, Boyd PW, Black EE, Siegel DA (2020) Metrics that matter for assessing the ocean biological carbon pump. Proc Natl Acad Sci USA 117:9679–9687
Buitenhuis ET, Rivkin RB, Sailley S, Le Quéré C (2010) Biogeochemical fluxes through microzooplankton. Global Biogeochem Cycles 24:GB4015
Butcher JC (2016) Numerical methods for ordinary differential equations. John Wiley & Sons
Caiger PE, Lefebve LS, Llopiz JK (2021) Growth and reproduction in mesopelagic fishes: a literature synthesis. ICES J Mar Sci 78:765–781
Calleja ML, Ansari MI, Røstad A, Silva L, Kaartvedt S, Irigoien X, Morán XAG (2018) The mesopelagic scattering layer: a hotspot for heterotrophic prokaryotes in the Red Sea twilight zone. Front Mar Sci 5:259
Calleja ML, Al-Otaibi N, Morán XAG (2019) Dissolved organic carbon contribution to oxygen respiration in the central Red Sea. Sci Rep 9:4690
Cavan EL, Hill SL (2022) Commercial fishery disturbance of the global ocean biological carbon sink. Glob Change Biol 28:1212–1221
Cherrier J, Valentine S, Hamill B, Jeffrey WH, Marra JF (2015) Light-mediated release of dissolved organic carbon by phytoplankton. J Mar Syst 147:45–51
Clarke T (1978) Diel feeding patterns of 16 species of mesopelagic fishes from Hawaiian waters. Fish Bull 76: 495–513
Crombet Y, Leblanc K, Quéguiner B, Moutin T and others (2011) Deep silicon maxima in the stratified oligotrophic Mediterranean Sea. Biogeosciences 8:459–475
Dalpadado P, Gjosaeter J (1987) Observations on mesopelagic fish from the Red Sea. Mar Biol 96:173–183
Dalpadado P, Gjøsæter J (1988) Feeding ecology of the lanternfish *Benthosema pterotum* from the Indian Ocean. Mar Biol 99:555–567
Davison PC, Checkley DM Jr, Koslow JA, Barlow J (2013) Carbon export mediated by mesopelagic fishes in the northeast Pacific Ocean. Prog Oceanogr 116:14–30
del Giorgio PA, Duarte CM (2002) Respiration in the open ocean. Nature 420:379–384
Dugdale RC, Goering JJ (1967) Uptake of new and regenerated forms of nitrogen in primary productivity. Limnol Oceanogr 12:196–206
Dypvik E, Kaartvedt S (2013) Vertical migration and diel feeding periodicity of the skinnycheek lanternfish (*Benthosema pterotum*) in the Red Sea. Deep Sea Res I 72: 9–16
Egge JK, Aksnes DL (1992) Silicate as regulating nutrient in phytoplankton competition. Mar Ecol Prog Ser 83: 281–289
Eppley RW, Peterson BJ (1979) Particulate organic matter flux and planktonic new production in the deep ocean. Nature 282:677–680
Furnas MJ (1990) *In situ* growth rates of marine phytoplankton: approaches to measurement, community and species growth rates. J Plankton Res 12:1117–1151
Getzlaff J, Oschlies A (2017) Pilot study on potential impacts of fisheries-induced changes in zooplankton mortality on marine biogeochemistry. Global Biogeochem Cycles 31: 1656–1673
Giering SLC, Sanders R, Martin AP, Lindemann C and others (2016) High export via small particles before the onset of the North Atlantic spring bloom. J Geophys Res Oceans 121:6929–6945
Honjo S, Eglinton TI, Taylor CD, Ulmer KM and others (2014) Understanding the role of the biological pump in the global carbon cycle: an imperative for ocean science. Oceanography 27:10–16
Huisman J, Pham Thi NN, Karl DM, Sommeijer B (2006) Reduced mixing generates oscillations and chaos in the oceanic deep chlorophyll maximum. Nature 439: 322–325
Irigoien X, Klevjer TA, Røstad A, Martinez U and others (2014) Large mesopelagic fishes biomass and trophic efficiency in the open ocean. Nat Commun 5:3271
Iserles A (2009) A first course in the numerical analysis of differential equations. No. 44. Cambridge University Press, New York, NY
Kaartvedt S, Staby A, Aksnes DL (2012) Efficient trawl avoidance by mesopelagic fishes causes large underestimation of their biomass. Mar Ecol Prog Ser 456:1–6
Kaartvedt S, Langbehn TJ, Aksnes DL (2019a) Enlightening the ocean's twilight zone. ICES J Mar Sci 76:803–812
Kaartvedt S, Røstad A, Opdal AF, Aksnes DL (2019b) Herding mesopelagic fish by light. Mar Ecol Prog Ser 625: 225–231
Kennedy CA, Carpenter MH (2019) Diagonally implicit Runge–Kutta methods for stiff ODEs. Appl Numer Math 146:221–244
Kheireddine M, Dall'Olmo G, Ouhssain M, Krokos G and others (2020) Organic carbon export and loss rates in the Red Sea. Global Biogeochem Cycles 34:e2020GB006650

Kinzer J, Schulz K (1985) Vertical distribution and feeding patterns of midwater fish in the central equatorial Atlantic. Mar Biol 85:313–322

Klevjer TA, Torres DJ, Kaartvedt S (2012) Distribution and diel vertical movements of mesopelagic scattering layers in the Red Sea. Mar Biol 159:1833–1841

Klevjer TA, Irigoien X, Røstad A, Fraile-Nuez E, Benítez-Barrios VM, Kaartvedt S (2016) Large scale patterns in vertical distribution and behaviour of mesopelagic scattering layers. Sci Rep 6:19873

Latasa M, Cabello AM, Morán XAG, Massana R, Scharek R (2017) Distribution of phytoplankton groups within the deep chlorophyll maximum. Limnol Oceanogr 62: 665–685

Liu Q, Zhou L, Wu Y, Huang H, He X, Gao N, Zhang L (2022) Quantification of the carbon released by a marine fish using a carbon release model and radiocarbon. Mar Pollut Bull 181:113908

López-Sandoval DC, Duarte CM, Agustí S (2021) Nutrient and temperature constraints on primary production and net phytoplankton growth in a tropical ecosystem. Limnol Oceanogr 66:2923–2935

Malviya S, Scalco E, Audic S, Vincent F and others (2016) Insights into global diatom distribution and diversity in the world's ocean. Proc Natl Acad Sci USA 113: E1516–E1525

Mariani G, Cheung WWL, Lyet A, Sala E and others (2020) Let more big fish sink: Fisheries prevent blue carbon sequestration — half in unprofitable areas. Sci Adv 6: eabb4848

Marsay CM, Sanders RJ, Henson SA, Pabortsava K, Achterberg EP, Lampitt RS (2015) Attenuation of sinking particulate organic carbon flux through the mesopelagic ocean. Proc Natl Acad Sci USA 112:1089–1094

Mazuecos IP, Aristegui J, Vázquez-Domínguez E, Ortega-Retuerta E, Gasol JM, Reche I (2015) Temperature control of microbial respiration and growth efficiency in the mesopelagic zone of the South Atlantic and Indian Oceans. Deep Sea Res I 95:131–138

Mazumder A, Taylor WD, McQueen DJ, Lean DRS (1990) Effects of fish and plankton on lake temperature and mixing depth. Science 247:312–315

Mitra A (2009) Are closure terms appropriate or necessary descriptors of zooplankton loss in nutrient–phytoplankton–zooplankton type models? Ecol Modell 220:611–620

Morán XAG, García FC, Røstad A, Silva L, Al-Otaibi N, Irigoien X, Calleja ML (2022) Diel dynamics of dissolved organic matter and heterotrophic prokaryotes reveal enhanced growth at the ocean's mesopelagic fish layer during daytime. Sci Total Environ 804:150098

Nowicki M, DeVries T, Siegel DA (2022) Quantifying the carbon export and sequestration pathways of the ocean's biological carbon pump. Global Biogeochem Cycles 36: e2021GB007083

Overmans S, Agustí S (2019) Latitudinal gradient of UV attenuation along the highly transparent Red Sea basin. Photochem Photobiol 95:1267–1279

Pinti J, Andersen KH, Visser AW (2021) Co-adaptive behavior of interacting populations in a habitat selection game significantly impacts ecosystem functions. J Theor Biol 523:110663

Proud R, Handegard NO, Kloser RJ, Cox MJ, Brierley AS (2019) From siphonophores to deep scattering layers: uncertainty ranges for the estimation of global mesopelagic fish biomass. ICES J Mar Sci 76:718–733

Qurban MA, Balala AC, Kumar S, Bhavya PS, Wafar M (2014) Primary production in the northern Red Sea. J Mar Syst 132:75–82

Radach G, Maier-Reimer E (1975) The vertical structure of phytoplankton growth dynamics — a mathematical model. Mém Soc R Sci Liège 6e Sér 7:113–146

Riley JS, Sanders R, Marsay C, Le Moigne FAC, Achterberg EP, Poulton AJ (2012) The relative contribution of fast and slow sinking particles to ocean carbon export. Global Biogeochem Cycles 26:GB1026

Robinson C (2019) Microbial respiration, the engine of ocean deoxygenation. Front Mar Sci 5:533

Roshan S, DeVries T (2017) Efficient dissolved organic carbon production and export in the oligotrophic ocean. Nat Commun 8:2036

Røstad A, Kaartvedt S, Aksnes DL (2016a) Erratum to 'Light comfort zones of mesopelagic acoustic scattering layers in two contrasting optical environments' [Deep-Sea Res. I 113 (2016) 1–6]. Deep Sea Res I 114:162–164

Røstad A, Kaartvedt S, Aksnes DL (2016b) Light comfort zones of mesopelagic acoustic scattering layers in two contrasting optical environments. Deep Sea Res I 113: 1–6

Saba GK, Burd AB, Dunne JP, Hernández-León S and others (2021) Toward a better understanding of fish-based contribution to ocean carbon flux. Limnol Oceanogr 66: 1639–1664

Sarmiento JL, Hughes TMC, Stouffer RJ, Manabe S (1998) Simulated response of the ocean carbon cycle to anthropogenic climate warming. Nature 393:245–249

Sarmiento JL, Slater R, Barber R, Bopp L and others (2004) Response of ocean ecosystems to climate warming. Global Biogeochem Cycles 18:GB3003

Sarnelle O (1993) Herbivore effects on phytoplankton succession in a eutrophic lake. Ecol Monogr 63:129–149

Seibel BA, Schneider JL, Kaartvedt S, Wishner KF, Daly KL (2016) Hypoxia tolerance and metabolic suppression in oxygen minimum zone euphausiids: implications for ocean deoxygenation and biogeochemical cycles. Integr Comp Biol 56:510–523

Silva L, Calleja ML, Huete-Stauffer TM, Ivetic S, Ansari MI, Viegas M, Morán XAG (2019) Low abundances but high growth rates of coastal heterotrophic bacteria in the Red Sea. Front Microbiol 9:3244

Sørnes TA, Aksnes DL (2004) Predation efficiency in visual and tactile zooplanktivores. Limnol Oceanogr 49:69–75

Steinberg DK, Landry MR (2017) Zooplankton and the ocean carbon cycle. Annu Rev Mar Sci 9:413–444

Stukel MR, Décima M, Landry MR (2022) Quantifying biological carbon pump pathways with a data-constrained mechanistic model ensemble approach. Biogeosciences 19:3595–3624

Svåsand T (1983) Populasjonsmodell for fisk med kort livssyklus med anvendelse på en tropisk myctophidae. MSc thesis, University of Bergen

Thingstad TF (2020) How trophic cascades and photic zone nutrient content interact to generate basin-scale differences in the microbial food web. ICES J Mar Sci 77: 1639–1647

Thingstad TF, Rassoulzadegan F (1999) Conceptual models for the biogeochemical role of the photic zone microbial food web, with particular reference to the Mediterranean Sea. Prog Oceanogr 44:271–286

Thingstad TF, Hagström Å, Rassoulzadegan F (1997) Accumulation of degradable DOC in surface waters: Is it

caused by a malfunctioning microbial loop? Limnol Oceanogr 42:398–404

Thingstad TF, Havskum H, Zweifel UL, Berdalet E and others (2007) Ability of a 'minimum' microbial food web model to reproduce response patterns observed in mesocosms manipulated with N and P, glucose, and Si. J Mar Syst 64:15–34

Thingstad TF, Våge S, Bratbak G, Egge J, Larsen A, Nejstgaard JC, Sandaa RA (2021) Reproducing the virus-to-copepod link in Arctic mesocosms using host fitness optimization. Limnol Oceanogr 66:303–313

Thornton DC (2014) Dissolved organic matter (DOM) release by phytoplankton in the contemporary and future ocean. Eur J Phycol 49:20–46

Torfstein A, Kienast SS, Yarden B, Rivlin A, Isaacs S, Shaked Y (2020) Bulk and export production fluxes in the Gulf of Aqaba, Northern Red Sea. ACS Earth Space Chem 4: 1461–1479

Tréguer P, Bowler C, Moriceau B, Dutkiewicz S and others (2018) Influence of diatom diversity on the ocean biological carbon pump. Nat Geosci 11:27–37

Turner JT (2015) Zooplankton fecal pellets, marine snow, phytodetritus and the ocean's biological pump. Prog Oceanogr 130:205–248

Vanni MJ, Layne CD, Arnott SE (1997) 'Top-down' trophic interactions in lakes: effects of fish on nutrient dynamics. Ecology 78:1–20

Wafar M, Qurban MA, Ashraf M, Manikandan KP, Flandez AV, Balala AC (2016) Patterns of distribution of inorganic nutrients in Red Sea and their implications to primary production. J Mar Syst 156:86–98

Wassmann P, Egge J, Reigstad M, Aksnes DL (1996) Influence of dissolved silicate on vertical flux of particulate biogenic matter. Mar Pollut Bull 33:10–21

Weikert H (1982) The vertical distribution of zooplankton in relation to habitat zones in the area of the Atlantis II Deep, Central Red Sea. Mar Ecol Prog Ser 8: 129–143

Wiebe PH, Bucklin A, Kaartvedt S, Røstad A, Blanco-Bercial L (2016) Vertical distribution and migration of euphausiid species in the Red Sea. J Plankton Res 38: 888–903

Wollrab S, Diehl S (2015) Bottom-up responses of the lower oceanic food web are sensitive to copepod mortality and feeding behavior. Limnol Oceanogr 60: 641–656

Wu J, Lee Z, Xie Y, Goes J and others (2021) Reconciling between optical and biological determinants of the euphotic zone depth. J Geophys Res Oceans 126: e2020JC016874

Zeldis JR, Décima M (2020) Mesozooplankton connect the microbial food web to higher trophic levels and vertical export in the New Zealand Subtropical Convergence Zone. Deep Sea Res I 155:103146

Editorial responsibility: Antonio Bode, A Coruña, Spain
Reviewed by: J. R. Zeldis and 1 anonymous referee

Submitted: March 16, 2023
Accepted: July 4, 2023
Proofs received from author(s): August 15, 2023